

STRUCTURAL ROBUSTNESS OF ELECTRIC MACHINE APPLICATIONS USING THE ICAD FRAMEWORK

Carlos E. Ugalde-Loo

Institute of Energy
Cardiff University
Wales, UK
Ugalde-LooC@cardiff.ac.uk

Eduardo Licéaga-Castro

CIIIA-FIME
UANL
México
e.liceaga.c@gmail.com

Luis A. Amézquita-Brooks

CIIIA-FIME
UANL
México
luis.amezquita@uanl.mx

Jesús Licéaga-Castro

Depto. de Electrónica
UAM-Azcapotzalco
México
ucastro21@hotmail.com

Abstract

Adequate control of three-phase machines (*e.g.*, induction motors -IMs- and synchronous generators -SGs-) is of paramount importance for the electric power industry. These are multivariable, non-linear systems. In this paper, it is formally demonstrated using the ICAD framework that the electrical subsystems of the IM and of the permanent magnet SG, due to their inherent structural robustness, are the multivariable equivalent to stable, minimum-phase, single-input single-output systems. As a consequence, an adequate performance and robustness may be achieved through fixed, stable, minimum-phase, diagonal controllers – justifying the widespread use of control schemes based on fixed, classical linear controllers such as PIs.

Key words

Decentralized control, frequency domain analysis and control, individual channel analysis and design, multivariable control, multivariable structure function.

1 Introduction

In a similar manner as the induction motor (IM) is the workhorse of the electric power industry when converting electrical into mechanical energy, the synchronous generator (SG) is the IM counterpart when transforming mechanical into electrical energy [Krause, Wasynczuk and Sudhoff, 2002]. Although both types of electric machines are fundamentally different, a common aspect shared by them is crucial to ensure their efficient utilization in industrial applications: an effective control, aiming at modifying the behavior of these three-phase machines to resemble that of a DC motor/generator. This is commonly achieved through vector (or field oriented) control schemes [Wu, 2006].

Such strategies are often based on fixed linear controllers (*e.g.*, PI structures) and are widely utilized [Vas, 1990] due to their simplicity and experimental success in electric machine applications –in detriment of more sophisticated techniques.

Three-phase electric machines such as the IM and the SG are non-linear multivariable systems [Krause, Wasynczuk and Sudhoff, 2002; Ugalde-Loo, Ekanayake and Jenkins, 2013]. It is noteworthy that fixed linear controllers are able to provide an adequate, robust performance in practice. In line with this, the structural robustness of two types of electric machines is here investigated. Through the individual channel analysis and design (ICAD) framework [O'Reilly and Leithead, 1991], it is shown that the electrical subsystems of the IM and the permanent magnet SG (PMSG) share characteristics that make them the multiple-input multiple-output (MIMO, or multivariable) equivalent of stable, minimum-phase, uncertain, single-input single-output (SISO) systems. Such attributes allow the use of fixed, stable, minimum-phase, diagonal controllers –and shed light on how is it possible that simple PI controllers are sufficient to operate specific machines.

2 Individual Channel Analysis and Design

In order to define the existence of stabilizing controllers for any system it is of great significance to assess its zero-pole structure, which may be affected by parametric uncertainty. The interpretation of such structure for multivariable systems, in terms of control design, is more difficult. ICAD, a frequency domain multivariable control framework, allows bridging this gap [O'Reilly and Leithead, 1991]. ICAD makes possible to analyze the existence of stabilizing controllers

through established SISO tools such as Bode/Nyquist plots and the Nyquist stability criterion. The ICAD set-up is described for 2×2 plants in this section. Extension to higher order systems is possible [Leithead and O'Reilly, 1992].

Let a 2×2 system be represented by

$$\mathbf{y}(s) = \mathbf{G}(s)\mathbf{u}(s), \quad (1)$$

$$\begin{bmatrix} y_1(s) \\ y_2(s) \end{bmatrix} = \begin{bmatrix} g_{11}(s) & g_{12}(s) \\ g_{21}(s) & g_{22}(s) \end{bmatrix} \begin{bmatrix} u_1(s) \\ u_2(s) \end{bmatrix},$$

where $g_{ij}(s)$ are scalar transfer functions, $y_i(s)$ the outputs, $u_i(s)$ the inputs and $r_i(s)$ the reference signals ($i, j = 1, 2$). Let a diagonal controller be defined as

$$\mathbf{u}(s) = \mathbf{K}(s)\mathbf{e}(s), \quad (2)$$

$$\begin{bmatrix} u_1(s) \\ u_2(s) \end{bmatrix} = \begin{bmatrix} k_1(s) & 0 \\ 0 & k_2(s) \end{bmatrix} \begin{bmatrix} e_1(s) \\ e_2(s) \end{bmatrix},$$

$$e_i(s) = r_i(s) - y_i(s),$$

The system (1)-(2) can be represented in terms of individual channels $c_i(s)$ relating $r_i(s)$ with $y_i(s)$:

$$c_i(s) = \frac{y_i(s)}{e_i(s)} = k_i(s)g_{ii}(s)(1 - \gamma(s)h_j(s)), \quad (3)$$

with $i \neq j$; $i, j = 1, 2$; where

$$\gamma(s) = \frac{g_{12}(s)g_{21}(s)}{g_{11}(s)g_{22}(s)} \quad (4)$$

is the *multivariable structure function (MSF)* and

$$h_i(s) = \frac{k_i(s)g_{ii}(s)}{1 + k_i(s)g_{ii}(s)}. \quad (5)$$

The cross-coupling relationship is given by

$$\frac{y_i(s)}{r_j(s)} = \frac{1}{1 + c_i(s)} \cdot \frac{g_{ij}(s)}{g_{jj}(s)} \cdot h_j(s) \quad (6)$$

$$= S_i(s) \cdot \frac{g_{ij}(s)}{g_{jj}(s)} \cdot h_j(s).$$

The previous representation entails no loss of information [Leithead and O'Reilly, 1992]. Figure 1 shows the block diagram of the system. Its equivalent scalar individual channels are given in Figure 2.

It has been shown in [Licéaga-Castro, Licéaga-Castro, Ugalde-Loo and Navarro-López, 2008] that the existence of stabilizing controllers of arbitrary high bandwidth depends on the individual channels (3), which are SISO plants. It is well-known that such controllers exist only when the system does not feature non-minimum phase zeros [Leithead and O'Reilly, 1991]. For the MIMO scenario, the existence of non-minimum phase transfer zeros has a similar role. The impact of transfer zeros of (1) can be assessed through an adequate interpretation of the MSF (4) by means of the Nyquist stability criterion. Detailed information can be found in [Licéaga-Castro, Licéaga-Castro and Ugalde-Loo, 2005].

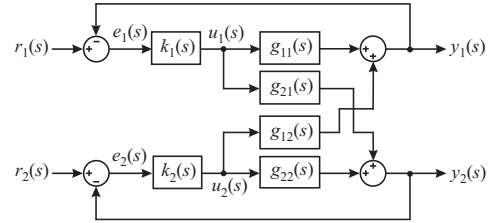


Figure 1. Block diagram representation with a diagonal controller.

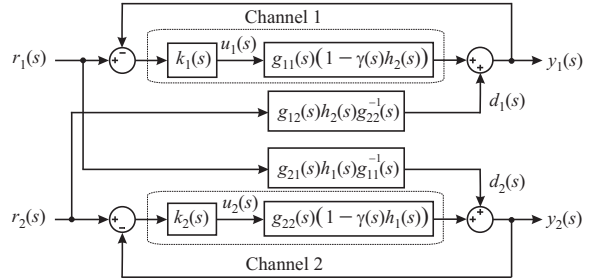


Figure 2. Equivalent individual channel representation.

There is an inherent relationship between the individual channels structure, their MSF and the MIMO transfer zeros. In fact, the sufficient conditions for (1) to have stable and minimum phase zero-pole individual channel configurations (3) are the following [O'Reilly and Leithead, 1991]:

- i. The system open loop poles are stable.
- ii. The MSF has no unstable poles.
- iii. The limit of $\gamma(s)$ as $s \rightarrow \infty$ is equal to zero.
- iv. The Nyquist plot of $\gamma(s)$ does not encircle the point $(1, 0)$.

In particular, conditions *ii* and *iv* are required for the transmission zeros to be minimum phase. However, this is not sufficient for the system to have integrity. If condition *ii* is not satisfied, the closed loop system may not possess integrity: compliance of condition *i* is also necessary for this. Condition *iii* is required so that arbitrary high-bandwidth control is possible.

If a system complies with all four conditions, the existence of a stabilizing controller (2) reduces to a controller that stabilizes simultaneously the individual channels (3) and the diagonal transfer functions (5) [O'Reilly and Leithead, 1991]. As $c_i(s)$ and $h_i(s)$ are stable and minimum phase, a system that complies with *i-iv* is the analogous of a stable and minimum phase SISO system, which may be controlled at an arbitrary bandwidth without incurring on unstable zero-pole cancellations. In addition, the resulting closed loop control system will also present integrity; *i.e.*, stability if either controller $k_1(s)$ or $k_2(s)$ is deactivated. This gives the system basic fault tolerance properties. It is possible to extend the previous attributes to uncertain MIMO systems represented as individual channels (*i.e.*, uncertain SISO systems).

Summarizing, it is possible to control a system complying with conditions *i-iv*, under parameter uncertainty and for realistic combinations of parameters, through fixed linear diagonal controllers. This is applicable, by extension, to more complex con-

rol structures. It is noteworthy that this is the simplest case within the ICAD framework. However, it is also possible to design stabilizing controllers even when none of the conditions i - iv are fulfilled [Licéaga-Castro, Licéaga-Castro and Ugalde-Loo, 2005; Licéaga-Castro, Licéaga-Castro, Ugalde-Loo and Navarro-López, 2008]. Further information on the ICAD framework can be found in [O'Reilly and Leithead, 1991; Leithead and O'Reilly, 1992].

3 Renewable Energy Technologies Application: the Permanent Magnet Synchronous Generator

Tidal stream and wind turbines (TSTs, WTs), along with other renewable energy technologies, are becoming considerably utilized in modern electrical power systems to mitigate climate change. They share some characteristics in terms of the electrical generators employed, system architecture and control strategies. In fact, both technologies aim to extract as much as possible energy from either the wind or the flow. Figure 3 shows the configuration of a turbine based on a PMSG and a full power converter applicable to wind and tidal stream turbines [Whitby and Ugalde-Loo, 2013].

The discussion in this paper is focused on the generator-side converter, which effectively controls the operation of the PMSG through the generator-side controller. Field oriented control schemes are typically employed for this [Anaya-Lara, Jenkins, Ekanayake, Cartwright and Hughes, 2009]. The scheme aims at decomposing the stator current into separate torque and field generating components (*i.e.*, resembling the operation of a DC machine) and requires an internal controller which decouples the stator currents (*i.e.*, the electrical subsystem). Further information on the complete control scheme may be found in [Krishnan, 2010].

Although the PMSG model is a multivariable, nonlinear system, the generator-side controller is normally designed using simplified SISO first order models. This practice may result in a control system with a limited performance that may require manual re-tuning. However, in this section it is formally shown that the PMSG has structural properties that allow the use of fixed, linear and low order controllers able to achieve system decoupling.

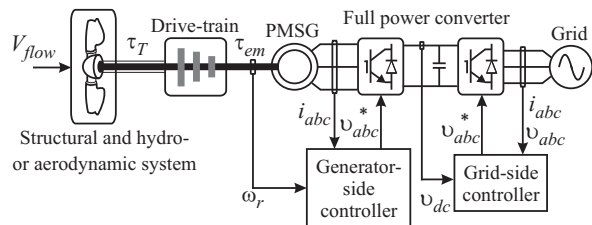


Figure 3. Wind/tidal stream turbine based on a PMSG [Whitby and Ugalde-Loo, 2013].

3.1 Mathematical Model

The PMSG model used for applications on renewable energy generation is expressed in a dq frame. It is described by [Krishnan, 2010]:

$$\begin{aligned}\frac{d}{dt}i_d &= \frac{v_d}{L_d} - \frac{R_s}{L_d}i_d + \frac{L_q}{L_d}n_P\omega_{gen}i_q, \\ \frac{d}{dt}i_q &= \frac{v_q}{L_q} - \frac{R_s}{L_q}i_q - \frac{L_d}{L_q}n_P\omega_{gen}i_d - \frac{\psi_m n_P \omega_{gen}}{L_q},\end{aligned}\quad (7)$$

where L_d, L_q , are the self inductances of the stator; R_s the stator resistance; v_d, v_q , the stator voltages; i_d, i_q , the stator currents; ψ_m the flux linkage of the permanent magnet; ω_{gen} the generator mechanical speed; $\omega_r = n_P\omega_{gen}$ the electrical rotor speed; and n_P the number of pole pairs. The model is completed by a suitable representation of the drive-train:

$$\begin{aligned}\frac{d}{dt}\omega_{gen} &= \frac{1}{J}(\tau_T - \tau_{em}), \\ \tau_{em} &= \frac{3}{2}n_P[\psi_m i_q + (L_d - L_q)i_d i_q],\end{aligned}\quad (8)$$

where J is the combined inertia of the rotor and generator, τ_T the hydro or aerodynamic torque developed by the rotor, and τ_{em} the electromagnetic torque.

Although system (7)-(8) is nonlinear, ω_{gen} varies at speeds well below the closed loop currents subsystem. This bandwidth separation allows considering ω_{gen} as an uncertain constant parameter when analyzing the currents subsystem. This is a well-known and accepted property of some nonlinear systems.

3.2 State-Space Representation

Let the PMSG be represented by (7) and (8). In vector control (or field oriented control) schemes, the generator-side converter controls the operation of the electric machine by effectively regulating the stator currents i_d, i_q , through the stator voltages v_d, v_q , in (7). The system has a state-space form

$$\begin{aligned}\dot{\mathbf{x}} &= \mathbf{A}\mathbf{x} + \mathbf{B}\mathbf{u}, \\ \mathbf{y} &= \mathbf{C}\mathbf{x} + \mathbf{D}\mathbf{u},\end{aligned}\quad (9)$$

where

$$\mathbf{x} = [i_d \ i_q]^T, \quad \mathbf{u} = [v_d \ v_q]^T, \quad \mathbf{y} = [i_d \ i_q]^T, \quad (10)$$

and

$$\mathbf{A} = \begin{bmatrix} -\frac{R_s}{L_d} & \frac{L_q}{L_d} \cdot n_P \omega_{gen} \\ -\frac{L_d}{L_q} \cdot n_P \omega_{gen} & -\frac{R_s}{L_q} \end{bmatrix}, \quad (11)$$

$$\mathbf{B} = \begin{bmatrix} \frac{1}{L_d} & 0 \\ 0 & \frac{1}{L_q} \end{bmatrix}, \quad \mathbf{C} = \begin{bmatrix} 1 & 0 \\ 0 & 1 \end{bmatrix}, \quad \mathbf{D} = \mathbf{0}_{2 \times 2}.$$

3.3 Transfer Matrix Representation

Although the system described by (7) and (8) is nonlinear, the generator mechanical speed ω_{gen} varies at

speeds considerably below the closed loop of the current subsystem. Due to such bandwidth separation, it is possible to consider (9)-(11) as linear time-invariant (LTI) and thus design a linear controller robust to parametric variations, with $\omega_{gen} \in [\omega_{gen,min}, \omega_{gen,max}]$ being the uncertain parameter. Thus, for a particular value of ω_{gen} , system (9) has a representation in the frequency domain as

$$\mathbf{y}(s) = \mathbf{G}_\omega(s)\mathbf{u}(s),$$

$$\begin{bmatrix} i_d(s) \\ i_q(s) \end{bmatrix} = \begin{bmatrix} g_{11}(s) & g_{12}(s) \\ g_{21}(s) & g_{22}(s) \end{bmatrix} \begin{bmatrix} v_d(s) \\ v_q(s) \end{bmatrix}, \quad (12)$$

where $\mathbf{G}_\omega(s) = \mathbf{C}(s\mathbf{I} - \mathbf{A})^{-1}\mathbf{B}$ is the transfer matrix. The elements of the transfer matrix are, explicitly,

$$\mathbf{G}_\omega(s) = \frac{\begin{bmatrix} L_q s + R_s & L_q n_P \omega_{gen} \\ -L_d n_P \omega_{gen} & L_d s + R_s \end{bmatrix}}{d_\omega(s)}$$

$$= \frac{\begin{bmatrix} n_{11}(s) & n_{12}(s) \\ n_{21}(s) & n_{22}(s) \end{bmatrix}}{d_\omega(s)}, \quad (13)$$

with

$$d_\omega(s) = L_d L_q s^2 + (L_d R_s + L_q R_s) s + R_s^2 + L_d L_q n_P^2 \omega_{gen}^2$$

$$= d_1 s^2 + d_2 s + d_3. \quad (14)$$

3.4 Individual Channel Analysis

System (12) conforms to the structure of a classical 2×2 ICAD system, and thus, the standard analysis and results from the ICAD framework apply directly. Conditions *i-iv* from Section 2 are proved to define the existence of stabilizing controllers for (13).

3.4.1 Condition *i*: the system is open loop stable:

Let

$$A = \{\mathbf{G}_\omega(s) : \omega_{gen} \in \mathbb{R}\} \quad (15)$$

be the set of transfer functions for every shaft speed ω_{gen} as defined by (13). The elements of set A are stable if and only if the poles of $\mathbf{G}_\omega(s)$ are stable; *i.e.*, $d_\omega(s)$ satisfies the Routh-Hurwitz stability criterion:

$$\text{Re}\{\text{poles}\{d_\omega(s)\}\} < 0 \Leftrightarrow \{d_1 > 0, d_2 > 0, d_3 > 0. \quad (16)$$

It is apparent from (14) that condition (16) is satisfied as $d_1 > 0$, $d_2 > 0$ and $d_3 > 0$ for realistic combinations of machine parameters (positive inductances and resistances). Therefore, A is open loop stable $\forall \omega_{gen}$. ■

3.4.2 Condition *ii*: the MSF is stable: Let the individual channels be defined as

$$c_1(s) : v_d(s) \rightarrow i_d(s)$$

$$c_2(s) : v_q(s) \rightarrow i_q(s). \quad (17)$$

The MSF is obtained according to (4) as follows:

$$\gamma_\omega(s) = \frac{g_{12}(s)g_{21}(s)}{g_{11}(s)g_{22}(s)} = -\frac{L_d L_q n_P^2 \omega_{gen}^2}{(L_q s + R_s)(L_d s + R_s)}. \quad (18)$$

Let

$$B = \{\gamma_\omega(s) : \omega_{gen} \in \mathbb{R}\} \quad (19)$$

be the resulting set of MSFs in (18). It is immediate that the elements of B are stable $\forall \omega_{gen}$ since the poles of $\gamma_\omega(s)$ are given by $\{-R_s/L_q, -R_s/L_d\}$ for any realistic combination of machine parameters. ■

3.4.3 Condition *iii*: the limit of $\gamma_\omega(s)$ as $s \rightarrow \infty$ is zero: Since the relative degree of (18) is 2, it is immediate that

$$\lim_{s \rightarrow \infty} \gamma_\omega(s) = 0. \quad (20)$$

3.4.4 Condition *iv*: the Nyquist plot of $\gamma_\omega(s)$ does not encircle (1, 0): Since condition *iii* is fulfilled, the Nyquist plot of $\gamma_\omega(s)$ does not encircle point (1, 0) if

$$\text{Re}\{\gamma_\omega(j\omega)\} < 1, \forall \omega \in E, \quad (21)$$

with

$$E = \{\omega : \arg[\gamma_\omega(j\omega)] = 0, \omega \in \mathbb{R}\}. \quad (22)$$

Thus, to satisfy condition *iv*, all the intersections of the Nyquist trajectory of $\gamma_\omega(s)$ with the real axis, represented by set E , should be to the left of (1, 0).

Evaluating the MSF (18) at $s = j\omega$ yields:

$$\gamma_\omega(j\omega) = \frac{-L_d L_q n_P^2 \omega_{gen}^2}{R_s^2 - L_d L_q \omega^2 + j(\omega L_d R_s + \omega L_q R_s)}, \quad (23)$$

which can be rewritten as:

$$\gamma_\omega(j\omega) = \frac{n_\gamma}{\text{re}_\gamma + j(\text{im}_\gamma)} = \frac{\text{re}_\gamma n_\gamma - j(\text{im}_\gamma n_\gamma)}{\text{re}_\gamma^2 + \text{im}_\gamma^2},$$

with $\text{re}_\gamma, \text{im}_\gamma \in \mathbb{R}$, and

$$n_\gamma = -L_d L_q n_P^2 \omega_{gen}^2, \quad \text{re}_\gamma = R_s^2 - L_d L_q \omega^2, \quad (24)$$

$$\text{im}_\gamma = \omega L_d R_s + \omega L_q R_s.$$

The real and imaginary parts of $\gamma_\omega(j\omega)$ are given by:

$$\text{Re}[\gamma_\omega(j\omega)] = \frac{\text{re}_\gamma n_\gamma}{\text{re}_\gamma^2 + \text{im}_\gamma^2},$$

$$\text{Im}[\gamma_\omega(j\omega)] = \frac{-\text{im}_\gamma n_\gamma}{\text{re}_\gamma^2 + \text{im}_\gamma^2}. \quad (25)$$

Set E is obtained by calculating the frequency values where the argument of $\gamma_\omega(j\omega)$ is equal to zero; *i.e.*,

$$\arg[\gamma_\omega(j\omega)] = 0 \Leftrightarrow \frac{\text{Im}[\gamma_\omega(j\omega)]}{\text{Re}[\gamma_\omega(j\omega)]} = \frac{-\text{im}_\gamma n_\gamma}{\text{re}_\gamma n_\gamma} = 0, \quad (26)$$

which is true if and only if $\text{re}_\gamma n_\gamma \rightarrow \pm\infty$ or $\text{im}_\gamma n_\gamma = 0$. Notice from (24) that

$$\begin{aligned} \text{re}_\gamma n_\gamma \rightarrow \infty &\Leftrightarrow \omega \rightarrow \pm\infty \quad \text{and} \\ \omega \rightarrow \pm\infty &\Rightarrow \gamma_\omega(j\omega) \rightarrow 0. \end{aligned}$$

Therefore, the elements of E are obtained by solving $\text{im}_\gamma n_\gamma = 0$ for ω . Thus condition (22) is rewritten as

$$E = \{\omega : \text{im}_\gamma n_\gamma = 0, \omega \in \mathbb{R}\}. \quad (27)$$

Elements of (27) are found using (24) as follows:

$$\text{im}_\gamma n_\gamma = -L_d L_q R_s n_p^2 \omega_{gen}^2 (L_d + L_q) \omega = 0, \quad (28)$$

from where it is obvious that $E = 0$, meaning that the only intersection of the Nyquist plot of $\gamma_\omega(j\omega)$ with the real axis (besides the origin) occurs at $\omega = 0$.

Using (25), condition (21) is rewritten as:

$$\text{Re}\{\gamma_\omega(j\omega)\} < 1 \Leftrightarrow \frac{\text{re}_\gamma n_\gamma}{\text{re}_\gamma^2 + \text{im}_\gamma^2} < 1. \quad (29)$$

Since $\text{re}_\gamma, \text{im}_\gamma \in \mathbb{R}$,

$$\frac{\text{re}_\gamma n_\gamma}{\text{re}_\gamma^2 + \text{im}_\gamma^2} < 1 \Leftrightarrow \text{re}_\gamma n_\gamma - (\text{re}_\gamma^2 + \text{im}_\gamma^2) < 0. \quad (30)$$

Evaluating (30) for $\omega = 0$ yields

$$\text{re}_\gamma n_\gamma - (\text{re}_\gamma^2 + \text{im}_\gamma^2) \Big|_{\omega=0} = -L_d L_q R_s^2 n_p^2 \omega_{gen}^2 - R_s^4. \quad (31)$$

It can be seen that

$$\text{Re}\{\gamma_\omega(j0)\} < 1 \Leftrightarrow -L_d L_q R_s^2 n_p^2 \omega_{gen}^2 - R_s^4 < 0, \quad (32)$$

which proves condition (21): the Nyquist plot of $\gamma_\omega(s)$ does not encircle the point (1, 0) for any realistic combination of parameters $\forall \omega_{gen} \in \mathbb{R}$. ■

4 High Performance Induction Motor Applications

IMs are widely used on industrial applications due to their attractive cost-effect attributes. However, for high performance applications such as high precision positioning, the operation of IMs is more complex than that of traditional DC motors. Within this context, the most successful control scheme is the rotor-flux indirect field oriented control (RIFOC) [Rodriguez, Kennel, Espinoza, Trincado, Silva and Rojas, 2012]. This is based on the introduction of torque- and flux-producing virtual stator currents. In this manner the IM can be operated as a DC motor. The scheme, shown in Figure 4, requires an internal controller which decouples the stator currents (or the electrical subsystem) [Amézquita-Brooks, Licéaga-Castro and Licéaga-Castro, 2013].

Although the IM is a MIMO non-linear system, the stator currents controller is normally designed using

simplified SISO first order models as in the case of the PMSG. Similarly, this results in control systems with limited performance requiring extensive manual tuning. In a similar fashion as in Section 3, it is formally demonstrated in this section that the IM has structural properties amenable to using fixed, linear, low order controllers for system decoupling.

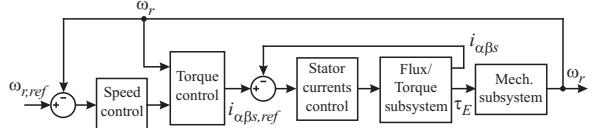


Figure 4. Traditional RIFOC IM control scheme.

4.1 Mathematical Model

The IM model is described by the following differential equations [Krishnan, 2001]:

$$\begin{aligned} \frac{d}{dt} i_{\alpha s} &= a_{11} i_{\alpha s} + \frac{L_m R_r}{\sigma L_s L_r^2} \psi_{\alpha r} + \frac{L_m \omega_r}{\sigma L_s L_r} \psi_{\beta r} + \frac{v_{\alpha s}}{\sigma L_s}, \\ \frac{d}{dt} i_{\beta s} &= a_{22} i_{\beta s} - \frac{L_m \omega_r}{\sigma L_s L_r} \psi_{\alpha r} + \frac{L_m R_r}{\sigma L_s L_r^2} \psi_{\beta r} + \frac{v_{\beta s}}{\sigma L_s}, \\ \frac{d}{dt} \psi_{\alpha r} &= \frac{L_m R_r}{L_r} i_{\alpha s} - \frac{R_r}{L_r} \psi_{\alpha r} - \omega_r \psi_{\beta r}, \\ \frac{d}{dt} \psi_{\beta r} &= \frac{L_m R_r}{L_r} i_{\beta s} + \omega_r \psi_{\alpha r} - \frac{R_r}{L_r} \psi_{\beta r}, \end{aligned} \quad (33)$$

where L_s, L_r, L_m , are the stator, rotor and mutual inductances; R_s, R_r , the stator and rotor resistances; $v_{\alpha s}, v_{\beta s}$, the stator voltages; $i_{\alpha s}, i_{\beta s}$, the stator currents; $\psi_{\alpha r}, \psi_{\beta r}$, the rotor fluxes; ω_r the electrical rotor speed; and

$$a_{11} = a_{22} = -\frac{L_r^2 R_s + L_m^2 R_r}{\sigma L_s L_r^2}.$$

The dispersion coefficient σ is defined as:

$$\sigma = 1 - \frac{L_m^2}{L_s L_r}. \quad (34)$$

Equations in (33) represent the electrical subsystem of the IM. The model is completed by

$$\begin{aligned} \frac{d}{dt} \omega_r &= \left(\frac{P}{2J} \right) (\tau_E - \tau_L), \\ \tau_E &= \frac{3}{2} \left(\frac{P}{2} \right) \frac{L_m}{L_r} (\psi_{\alpha r} i_{\beta s} - \psi_{\beta r} i_{\alpha s}), \end{aligned} \quad (35)$$

where J is the rotor inertia, τ_L the load torque, τ_E the electromagnetic torque, and P the number of poles.

As in the case of the PMSG, although system (33)-(35) is nonlinear, ω_r varies at speeds well below the closed loop currents subsystem. This bandwidth separation allows considering ω_r as an uncertain constant parameter when analyzing the currents subsystem.

4.2 State-Space Representation

Let an IM be represented by (33) and (35). Vector control schemes require the control of the stator currents $i_{\alpha s}$, $i_{\beta s}$, by driving the stator voltages $v_{\alpha s}$, $v_{\beta s}$, using a voltage source inverter. The system has a state-space representation (9), where

$$\begin{aligned} \mathbf{x} &= [i_{\alpha s} \ i_{\beta s} \ \psi_{\alpha r} \ \psi_{\beta r}]^T, \\ \mathbf{u} &= [v_{\alpha s} \ v_{\beta s}]^T, \\ \mathbf{y} &= [i_{\alpha s} \ i_{\beta s}]^T, \end{aligned} \quad (36)$$

and

$$\mathbf{A} = \begin{bmatrix} a_{11} & 0 & \frac{L_m R_r}{\sigma L_s L_r^2} & \frac{L_m \omega_r}{\sigma L_s L_r} \\ 0 & a_{22} & -\frac{L_m \omega_r}{\sigma L_s L_r} & \frac{L_m R_r}{\sigma L_s L_r^2} \\ \frac{L_m R_r}{L_r} & 0 & -\frac{R_r}{L_r} & -\omega_r \\ 0 & \frac{L_m R_r}{L_r} & \omega_r & -\frac{R_r}{L_r} \end{bmatrix},$$

$$\mathbf{B} = \begin{bmatrix} \frac{1}{\sigma L_s} & 0 & 0 & 0 \\ 0 & \frac{1}{\sigma L_s} & 0 & 0 \end{bmatrix}^T, \quad \mathbf{C} = \begin{bmatrix} 1 & 0 & 0 & 0 \\ 0 & 1 & 0 & 0 \end{bmatrix}, \quad \mathbf{D} = \mathbf{0}_{2 \times 2}.$$

(37)

4.3 Transfer Matrix Representation

The stator currents subsystem of the IM is a nonlinear plant. However, it is possible to consider the realization (9), (36), (37) as LTI since the rotor speed ω_r varies at speeds considerably below the closed loop of the current subsystem. Such a bandwidth separation allows the design of a linear controller robust to parametric variations, with $\omega_r \in [\omega_{r,min}, \omega_{r,max}]$ being the uncertain parameter.

Following the same procedure as in Section 3, the system is represented in the frequency domain for particular values of ω_r as

$$\begin{aligned} \mathbf{y}(s) &= \mathbf{G}_{\omega_r}(s) \mathbf{u}(s), \\ \begin{bmatrix} i_{\alpha s}(s) \\ i_{\beta s}(s) \end{bmatrix} &= \begin{bmatrix} g_{11}(s) & g_{12}(s) \\ g_{21}(s) & g_{22}(s) \end{bmatrix} \begin{bmatrix} v_{\alpha s}(s) \\ v_{\beta s}(s) \end{bmatrix}, \end{aligned} \quad (38)$$

with

$$\mathbf{G}_{\omega_r}(s) = \frac{\begin{bmatrix} n_{\omega_r,11}(s) & n_{\omega_r,12}(s) \\ n_{\omega_r,21}(s) & n_{\omega_r,22}(s) \end{bmatrix}}{d_{\omega_r}(s)}, \quad (39)$$

Elements of (39) are given as

$$\begin{aligned} n_{\omega_r,11}(s) &= n_{\omega_r,22}(s) = \frac{1}{\sigma L_s} \cdot \dots \\ &= \left[\left(s^3 + \frac{2\sigma L_s L_r^2 R_r + L_m^2 R_r L_r + L_r^3 R_s}{\sigma L_s L_r^3} s^2 \right) + \right. \\ &+ \left. \left(\frac{\sigma L_s L_r (L_r^2 \omega_r^2 + R_r^2) + 2L_r^2 R_s R_r + L_m^2 R_r^2}{\sigma L_s L_r^3} s \right) + \right. \\ &+ \left. \left(\frac{L_r^3 R_s \omega_r^2 + L_r R_s R_r^2}{\sigma L_s L_r^3} \right) \right], \\ n_{\omega_r,12}(s) &= -n_{\omega_r,21}(s) = -\frac{L_m^2 R_r \omega_r}{\sigma^2 L_s^2 L_r^2} s, \\ d_{\omega_r}(s) &= s^4 + d_{\omega_1} s^3 + d_{\omega_2} s^2 + d_{\omega_3} s + d_{\omega_4}, \end{aligned} \quad (40)$$

with

$$\begin{aligned} d_{\omega_1} &= \kappa (2\sigma L_s L_r^2) (L_m^2 R_r + \sigma L_s L_r R_r + L_r^2 R_s), \\ d_{\omega_2} &= \kappa [L_m^4 R_r^2 + L_r^4 R_s^2 + \sigma^2 L_s^2 L_r^2 (R_r^2 + L_r^2 \omega_r^2)] + \\ &+ \kappa [2L_r^2 L_m^2 R_s R_r + 2\sigma L_s L_r R_r (2L_r^2 R_s + L_m^2 R_r)], \\ d_{\omega_3} &= 2\kappa L_r R_s R_r (L_r^2 R_s + L_m^2 R_r) + \\ &+ 2\kappa \sigma L_s L_r^2 R_s (R_r^2 + L_r^2 \omega_r^2), \\ d_{\omega_4} &= \kappa (L_r^4 R_s^2 \omega_r^2 + L_r^2 R_s^2 R_r^2), \\ \kappa &= (\sigma^2 L_s^2 L_r^4)^{-1} \end{aligned} \quad (41)$$

4.4 Individual Channel Analysis

System (38) also conforms to the structure of a classical 2×2 ICAD system. Conditions *i-iv* from Section 2 are proved in a similar way as in Section 3.

4.4.1 Condition *i*: the system is open loop stable: Let

$$C = \{ \mathbf{G}_{\omega_r}(s) : \omega_r \in \mathbb{R} \} \quad (42)$$

be the set of transfer functions for every mechanical speed ω_r as defined by (39). The elements of C are stable if and only if the poles of $\mathbf{G}_{\omega_r}(s)$ are stable. This requires that the real part of the roots of $d_{\omega_r}(s)$ in (40) satisfy the Routh-Hurwitz stability criterion; *i.e.*,

$$\begin{aligned} \text{Re}\{\text{poles}\{d_{\omega_r}(s)\}\} &< 0 \Leftrightarrow \\ \begin{cases} d_{\omega_1} > 0, d_{\omega_2} > 0, d_{\omega_3} > 0, \\ d_{\omega_4} > 0, d_{\omega_1} d_{\omega_2} - d_{\omega_3} > 0, \\ d_{\omega_1} d_{\omega_2} d_{\omega_3} - d_{\omega_3}^2 - d_{\omega_1}^2 d_{\omega_4} > 0. \end{cases} \end{aligned} \quad (43)$$

From (34) it can be seen that $\sigma > 0$ for any realistic combination of inductances (positive values), since $L_s = L_{ls} + L_m$ and $L_r = L_{lr} + L_m$, where L_{ls} and L_{lr} are the stator and rotor leakage inductances. Thus, it is clear from (41) that $d_{\omega_1} > 0$, $d_{\omega_2} > 0$, $d_{\omega_3} > 0$, and $d_{\omega_4} > 0$ for realistic combinations of machine parameters (positive inductances and resistances). It can be shown that

$$d_{\omega 1} d_{\omega 2} - d_{\omega 3} = \frac{2(L_r R_s + L_s R_r)^3}{\mu^3} + \frac{2L_s R_r \omega_r^2}{\mu} + \frac{2R_r R_s (L_r R_s + L_s R_r)}{\mu^2},$$

$$d_{\omega 1} d_{\omega 2} d_{\omega 3} - d_{\omega 3}^2 - d_{\omega 1}^2 d_{\omega 4} = 4R_r R_s \cdot \dots [\omega_r^2 \mu^2 + (L_r R_s + L_s R_r)^2] \mu^{-5} \cdot \dots [\mu L_s L_r \omega_r^2 + (L_r R_s + L_s R_r)^2], \quad (44)$$

where $\mu = L_s L_r - L_m^2$. Since $\sigma > 0 \Rightarrow \mu > 0$,

$$d_{\omega 1} d_{\omega 2} - d_{\omega 3} > 0 \text{ and} \quad (45)$$

$$d_{\omega 1} d_{\omega 2} d_{\omega 3} - d_{\omega 3}^2 - d_{\omega 1}^2 d_{\omega 4} > 0.$$

Therefore, C is open loop stable for any realistic combination of machine parameters $\forall \omega_r$. ■

4.4.2 Condition ii: the MSF is stable: Let the individual channels be defined as

$$c_1(s) : v_{\alpha s}(s) \rightarrow i_{\alpha s}(s) \quad (46)$$

$$c_2(s) : v_{\beta s}(s) \rightarrow i_{\beta s}(s).$$

The MSF is obtained according to (4), (39), and (40) as follows:

$$\gamma_{\omega r}(s) = \frac{g_{12}(s)g_{21}(s)}{g_{11}(s)g_{22}(s)} = - \left[\frac{n_{\omega r,12}(s)}{n_{\omega r,11}(s)} \right]^2. \quad (47)$$

For convenience, $n_{\omega r,11}(s)$ in (40) is rewritten as

$$n_{\omega r,11}(s) = \eta_1 s^3 + \eta_2 s^2 + \eta_3 s + \eta_4, \quad (48)$$

with

$$\eta_1 = \frac{1}{\sigma L_s}, \quad \eta_2 = \frac{2\sigma L_s L_r^2 R_r + L_m^2 R_r L_r + L_r^3 R_s}{\sigma^2 L_s^2 L_r^3},$$

$$\eta_3 = \frac{\sigma L_s L_r^3 \omega_r^2 + 2L_r^2 R_s R_r + \sigma L_s L_r R_r^2 + L_m^2 R_r^2}{\sigma^2 L_s^2 L_r^3},$$

$$\eta_4 = \frac{L_r^3 R_s \omega_r^2 + L_r R_s R_r^2}{\sigma^2 L_s^2 L_r^3}. \quad (49)$$

Let

$$D = \{\gamma_{\omega r}(s) : \omega_r \in \mathbb{R}\} \quad (50)$$

be the resulting set of MSFs in (47). The elements of D are stable if and only if the poles of $\gamma_{\omega r}(s)$ satisfy the Routh-Hurwitz criterion $\forall \omega_r$. That is,

$$\text{Re}\{\text{poles}\{\gamma_{\omega r}(s)\}\} < 0 \Leftrightarrow$$

$$\begin{cases} \eta_1 > 0, \eta_2 > 0, \eta_3 > 0, \\ \eta_4 > 0, \eta_2 \eta_3 - \eta_1 \eta_4 > 0. \end{cases} \quad (51)$$

It can be noticed from (49) that $\eta_1 > 0, \eta_2 > 0, \eta_3 > 0, \eta_4 > 0$ for realistic combinations of IM parameters. Further algebraic manipulation shows that

$$\eta_2 \eta_3 - \eta_1 \eta_4 = \beta (3L_r^2 L_m^2 R_s R_r^2 + L_m^4 R_r^3) + \beta (4\sigma L_s L_r^3 R_s R_r^2 + 3\sigma L_s L_r L_m^2 R_r^3 + 2L_r^4 R_s^2 R_r) + \beta [\omega_r^2 \sigma L_s L_r^3 R_r (2\sigma L_s L_r + L_m^2) + 2\sigma^2 L_s^2 L_r^2 R_r^3], \quad (52)$$

where $\beta = (\sigma^4 L_s^4 L_r^5)^{-1}$. It is clear that

$$\eta_2 \eta_3 - \eta_1 \eta_4 > 0 \quad (53)$$

$\forall \omega_r$. Therefore, set D is stable $\forall \omega_r$ for any realistic combination of machine parameters. ■

4.4.3 Condition iii: the limit of $\gamma_{\omega r}(s)$ as $s \rightarrow \infty$ is zero: As in the case of a PMSG, the proof for an IM is immediate, since it can be seen from (40) and (47) that the relative degree of $\gamma_{\omega r}(s)$ is 4. ■

4.4.4 Condition iv: the Nyquist plot of $\gamma_{\omega r}(s)$ does not encircle $(1, 0)$: Since condition iii is fulfilled, the Nyquist plot of $\gamma_{\omega r}(s)$ does not encircle the point $(1, 0)$ if

$$\text{Re}\{\gamma_{\omega r}(j\omega)\} < 1, \forall \omega \in F \quad (54)$$

with

$$F = \{\omega : \arg[\gamma_{\omega r}(j\omega)] = 0, \omega \in \mathbb{R}\}. \quad (55)$$

This requires that all the intersections of the Nyquist trajectory of $\gamma_{\omega r}(s)$ with the real axis, represented by F , should be to the left of $(1, 0)$. Following some algebraic manipulation and by using (40), the MSF (47), evaluated at $s = j\omega$, is given as:

$$\gamma_{\omega r}(j\omega) = \frac{L_r^2 L_m^4 R_r^2 \omega_r^2 \omega^2}{d_{\gamma \omega}^2}, \quad (56)$$

where

$$d_{\gamma \omega} = -j\omega \sigma L_s L_r^3 \omega_r^2 - L_r^3 R_s \omega_r^2 + j\omega^3 \sigma L_s L_r^3 + 2\omega^2 \sigma L_s L_r^2 R_r - j\omega \sigma L_s L_r R_r^2 + \omega^2 L_r^3 R_s + -2j\omega L_r^2 R_s R_r - L_r R_s R_r^2 + \omega^2 L_r L_m^2 R_r + -j\omega L_m^2 R_r^2,$$

which in turn is rewritten as

$$d_{\gamma \omega} = \text{re}_{d\gamma} + j(\text{im}_{d\gamma})$$

to facilitate the analysis, with $\text{re}_{d\gamma}, \text{im}_{d\gamma} \in \mathbb{R}$, and

$$\text{re}_{d\gamma} = -L_r^3 R_s \omega_r^2 + 2\omega^2 \sigma L_s L_r^2 R_r + \omega^2 L_r^3 R_s + -L_r R_s R_r^2 + \omega^2 L_r L_m^2 R_r,$$

$$\text{im}_{d\gamma} = -\omega \sigma L_s L_r^3 \omega_r^2 + \omega^3 \sigma L_s L_r^3 - \omega \sigma L_s L_r R_r^2 + -2\omega L_r^2 R_s R_r - \omega L_m^2 R_r^2. \quad (57)$$

Therefore $\gamma_{\omega r}(j\omega)$ in (56) can be expressed as:

$$\gamma_{\omega r}(j\omega) = \frac{L_r^2 L_m^4 R_r^2 \omega_r^2 \omega^2 \zeta}{(\text{re}_{d\gamma}^2 - \text{im}_{d\gamma}^2)^2 + (2\text{re}_{d\gamma} \text{im}_{d\gamma})^2}, \quad (58)$$

which was obtained after realizing the denominator, where

$$\zeta = \left[(\text{re}_{d\gamma}^2 - \text{im}_{d\gamma}^2) - 2j(\text{re}_{d\gamma} \text{im}_{d\gamma}) \right].$$

Separating (58) into real and imaginary components yields

$$\text{Re}[\gamma_{\omega r}(j\omega)] = \frac{L_r^2 L_m^4 R_r^2 \omega_r^2 \omega^2 (\text{re}_{d\gamma}^2 - \text{im}_{d\gamma}^2)}{(\text{re}_{d\gamma}^2 - \text{im}_{d\gamma}^2)^2 + (2\text{re}_{d\gamma} \text{im}_{d\gamma})^2}, \quad (59)$$

$$\text{Im}[\gamma_{\omega r}(j\omega)] = \frac{-L_r^2 L_m^4 R_r^2 \omega_r^2 \omega^2 (2\text{re}_{d\gamma} \text{im}_{d\gamma})}{(\text{re}_{d\gamma}^2 - \text{im}_{d\gamma}^2)^2 + (2\text{re}_{d\gamma} \text{im}_{d\gamma})^2}, \quad (60)$$

For simplicity, let

$$c_1 = \text{re}_{d\gamma}^2 - \text{im}_{d\gamma}^2, \quad c_2 = 2\text{re}_{d\gamma} \text{im}_{d\gamma}, \quad (61)$$

with $c_1, c_2 \in \mathbb{R}$. Thus,

$$\text{Re}[\gamma_{\omega r}(j\omega)] = \frac{L_r^2 L_m^4 R_r^2 \omega_r^2 \omega^2 c_1}{c_1^2 + c_2^2}, \quad (62)$$

$$\text{Im}[\gamma_{\omega r}(j\omega)] = \frac{-L_r^2 L_m^4 R_r^2 \omega_r^2 \omega^2 c_2}{c_1^2 + c_2^2}. \quad (63)$$

Using (62), condition (54) may be rewritten as

$$\frac{L_r^2 L_m^4 R_r^2 \omega_r^2 \omega^2 c_1}{c_1^2 + c_2^2} < 1, \forall \omega \in F. \quad (64)$$

Since $c_1, c_2 \in \mathbb{R}$,

$$\frac{L_r^2 L_m^4 R_r^2 \omega_r^2 \omega^2 c_1}{c_1^2 + c_2^2} < 1 \Leftrightarrow L_r^2 L_m^4 R_r^2 \omega_r^2 \omega^2 c_1 < c_1^2 + c_2^2 \quad (65)$$

It can be seen that for $c_1 < 0$, inequality (65) holds $\forall \omega \in F$. This is sufficient to prove condition *iv*. However, if $c_1 > 0$, then (65) is equivalent to

$$\frac{L_r^2 L_m^4 R_r^2 \omega_r^2 \omega^2 c_1}{c_1^2 + c_2^2} < 1 \Leftrightarrow c_1 + \frac{c_2^2}{c_1} - L_r^2 L_m^4 R_r^2 \omega_r^2 \omega^2 > 0 \quad (66)$$

In order to prove (65) and (66) it is necessary to calculate set F defined by (55); *i.e.*, the frequency values ω at which the argument of $\gamma_{\omega r}(s)$ is equal to zero. From (62) and (63),

$$\arg[\gamma_{\omega r}(j\omega)] = 0 \Leftrightarrow \frac{\text{Im}[\gamma_{\omega r}(j\omega)]}{\text{Re}[\gamma_{\omega r}(j\omega)]} = \frac{-c_2}{c_1} = 0, \quad (67)$$

which is true if and only if $c_1 \rightarrow \pm\infty$ and/or $c_2 = 0$. Considering, by condition *iii*, that

$$c_1 \rightarrow \pm\infty \Leftrightarrow \omega \rightarrow \pm\infty \quad \text{and} \\ \omega \rightarrow \pm\infty \Rightarrow \gamma_{\omega r}(j\omega) \rightarrow 0,$$

then the elements of F are the roots of c_2 . That is,

$$F = \{\omega : c_2 = 0, \omega \in \mathbb{R}\}. \quad (68)$$

Elements of (68) are found using (61) and (57) as

$$F = \{F(1), F(2), F(3)\}, \quad (69)$$

with

$$F(1) = 0, \quad F(2) = \pm \frac{\sqrt{\Omega(R_r^2 + \omega_r^2 L_r^2)} R_s}{\Omega}, \\ F(3) = \pm \frac{\sqrt{\Psi[\Psi(\omega_r^2 L_r^2 + R_r^2) + \Upsilon]}}{\Psi^2}.$$

and

$$\Omega = 2\sigma L_s L_r R_r + L_r^2 R_s + L_m^2 R_r, \\ \Psi = \sigma L_s L_r, \\ \Upsilon = 2L_r R_s R_r + L_m^2 R_r^2.$$

Since

$$\text{Re}\{\gamma_{\omega r}(j\omega)\} = \text{Re}\{\gamma_{\omega r}(-j\omega)\} \quad \forall \omega \in \mathbb{R}^+,$$

only positive values of ω in set F described by (69) are tested in condition (54). If $\omega = F(1)$, it follows directly from (56) that

$$\gamma_{\omega r}(j\omega) = 0 \Rightarrow \text{Re}\{\gamma_{\omega r}(jF(1))\} < 1. \quad (70)$$

If $\omega = F(2)$, c_1 is calculated using (57) and (61) as:

$$c_1 = \frac{-R_s [R_r^4 + (R_r \omega_r L_r)^2]}{(2\sigma L_s L_r R_r + L_r^2 R_s + L_m^2 R_r)^3} \cdot c_{1\alpha}, \quad (71)$$

where

$$c_{1\alpha} = [L_m^4 R_r^2 + 3\sigma L_s L_r L_m^2 R_r^2 + 3L_r^2 L_m^2 R_s R_r + \\ + L_s L_r^3 L_m^2 \sigma \omega_r^2 + 2(\sigma L_s L_r R_r)^2 + 2L_r^4 R_s^2 + \\ + 4\sigma L_s L_r^3 R_s R_r + 2L_r^4 (\sigma L_s \omega_r)^2]^2. \quad (72)$$

It is obvious that $c_{1\alpha} > 0$, and therefore, $c_1 < 0$ for any realistic combination of machine parameters. From (65), it follows that

$$c_1 < 0 \Rightarrow \text{Re}\{\gamma_{\omega r}(jF(2))\} < 1. \quad (73)$$

If $\omega = F(3)$, c_1 is obtained as

$$c_1 = \frac{R_r^2}{\sigma^2 L_s^2 L_r^4} \cdot c_{1\alpha}. \quad (74)$$

Since $c_{1\alpha} > 0$, from (74) it follows that $c_1 > 0$. In this case, the inequality defined in (66) is checked; that is,

$$\text{Re}\{\gamma_{\omega r}(jF(3))\} < 1 \Leftrightarrow c_1 + \frac{c_2^2}{c_1} - L_r^2 L_m^4 R_r^2 \omega_r^2 \omega^2 > 0 \quad (75)$$

Algebraic calculation for $\omega = F(3)$ gives

$$\begin{aligned}
c_1 + \frac{c_2^2}{c_1} - L_r^2 L_m^4 R_r^2 \omega_r^2 \omega^2 &= \frac{R_r^2}{\sigma^2 L_s^2 L_r^4} \\
&\cdot [L_r^4 R_s^2 + 2L_r^2 L_m^2 R_s R_r + L_m^4 R_r^2 + \dots \\
&+ \sigma L_s L_r (L_r^2 L_m^2 \omega_r^2 + 2L_r^2 R_s R_r + 2L_m^2 R_r^2) + \dots \\
&+ L_r^4 (\sigma L_s \omega_r)^2 + (\sigma L_s L_r R_r)^2] \\
&\cdot [4L_r^4 R_s^2 + 4L_r^2 L_m^2 R_s R_r + L_m^4 R_r^2 + \dots \\
&+ 8\sigma L_s L_r^3 R_s R_r + 4\sigma L_s L_r L_m^2 R_r^2 + \dots \\
&+ 4L_r^4 (\sigma L_s \omega_r)^2 + 4(\sigma L_s L_r R_r)^2]
\end{aligned}$$

which shows that (75) is fulfilled.

Since (70), (73) and (75) are true, condition (54) has been proven: the Nyquist plot of $\gamma_{\omega_r}(s)$ does not encircle the point $(1, 0) \forall \omega_r \in \mathbb{R}$ for any realistic combination of IM machine parameters. ■

5 Discussion and Concluding Remarks

The mathematical proofs presented in Sections 3 and 4, namely that the PMSG and the IM comply with conditions *i-iv*, show that the existence of a diagonal stabilizing controller for either machine reduces to the existence of a controller which simultaneously stabilizes the individual channels and the diagonal transfer functions. As in both cases the channels and the diagonal transfer functions are stable and minimum phase, the systems may be controlled at an arbitrary bandwidth without incurring on unstable zero/pole cancellations.

Compliance of conditions *i-iv* for all realistic combinations of system parameters is a consequence of the inherent structural robustness of the PMSG and the IM. These attributes shed some light as to why simple diagonal stabilizing controllers are able to achieve an adequate system performance under parametric variations—in both cases, the rotor speed.

Although the studies here presented are based on a simple diagonal control structure, the results can be generalized to more complex structures by extension.

References

- Amézquita-Brooks, L., Licéaga-Castro, J. and Licéaga-Castro, E. (2013). Speed and Position Controllers Using Indirect Field Oriented Control: A Classical Control Approach. *IEEE Transactions on Industrial Electronics*, in press.
- Anaya-Lara, O., Jenkins, N., Ekanayake, J. B., Cartwright, P. and Hughes, M. (2009). *Wind Energy Generation. Modelling and Control*. John Wiley and Sons, UK.
- Krause, P. C., Wasynczuk, O. and Sudhoff, S. D. (2002). *Analysis of Electric Machinery and Drive Systems*. Wiley-IEEE Press, USA.
- Krishnan, R. (2001). *Electric Motor Drives: Modeling, Analysis, and Control*. Prentice Hall, USA.
- Krishnan, R. (2010). *Permanent Magnet Synchronous and Brushless DC Motor Drives*. Taylor & Francis.
- Leithead, W. E. and O'Reilly, J. (1991). Uncertain SISO systems with fixed stable minimum-phase controllers: rela-

- tionship of closed-loop systems to plant RHP poles and zeros. *International Journal of Control*, **53**(4), pp. 771–798.
- Leithead, W. E. and O'Reilly, J. (1992). M-Input m-output Feedback Control by Individual Channel Design. Part 1. Structural Issues. *International Journal of Control*, **56**(6), pp. 1347–1397.
- Licéaga-Castro, E., Licéaga-Castro, J. and Ugalde-Loo, C. E. (2005). Beyond the Existence of Diagonal Controllers: from the Relative Gain Array to the Multivariable Structure Function. In *44th IEEE Conference on Decision and Control, and European Control Conference (CDC-ECC)*, Sevilla, Spain, Dec. 12–15, pp. 7150–7156.
- Licéaga-Castro, E., Licéaga-Castro, J., Ugalde-Loo, C. E. and Navarro-López, E. M. (2008). Efficient multivariable submarine depth-control system design. *Ocean Engineering*, **35**(17–18), pp. 1747–1758.
- O'Reilly, J. and Leithead, W. E. (1991). Multivariable control by 'individual channel design'. *International Journal of Control*, **54**(1), pp. 1–46.
- Rodriguez, J., Kennel, R. M., Espinoza, J. R., Trincado, M., Silva, C. A. and Rojas, C. A. (2012). High-Performance Control Strategies for Electrical Drives: An Experimental Assessment. *IEEE Transactions on Industrial Electronics*, **59**(2), pp. 812–820.
- Ugalde-Loo, C. E., Ekanayake, J. B. and Jenkins, N. (2013). State-Space Modeling of Wind Turbine Generators for Power System Studies. *IEEE Transactions on Industry Applications*, **49**(1), pp. 223–232.
- Vas, P. (1990). *Vector Control of AC Machines*. Oxford University Press, USA.
- Whitby, B. and Ugalde-Loo, C. E. (2013). Performance of Pitch and Stall Regulated Tidal Stream Turbines. *IEEE Transactions on Sustainable Energy*, in press.
- Wu, B. (2006). *High-Power Converters and AC Drives*. Wiley-IEEE Press, USA.